LMedS-Based Power Regression: An Optimal and Automatic Method of Radiometric Intercalibration for DMSP-OLS NTL Imagery

Chang Li, Xi Li, Tian Li, Qi Meng, and Wenjie Yu

***Abstract*—The further scientific applications of DMSP-OLS night-time light (NTL) imagery have been being limited by the accuracy, automation, and speed of radiometric intercalibration. In order to solve the aforementioned problems, this article is the first to propose a new least-median-of-squares (LMedS)-based power regression (LBPR) for automatically radiometric intercalibration and investigate the reasons for the optimal model of radiometric intercalibration, especially those based on the Taylor expansion and probability principle. NTL data in six regions all over the world, from 1994 and 1997 to 2007, were used as the test datasets. When the five kinds of LMedS-based radiometric intercalibration models (i.e., linear, quadratic, power, exponential, and logarithmic regression) are synthetically compared in absolute accuracy (adjusted RMSE) and running speed, it is concluded that the LBPR, which has the highest accuracy and preferable running speed, is recommended as the optimal method, which can also be used as a reference for other types of imagery preprocessing.**

***Index Terms*—Accuracy, adjusted root-mean-square error (RMSE), automation, defense meteorological satellite program operational linescan system (DMSP-OLS) night-time light (NTL) imagery, least median of squares (LMedS)-based power regression (LBPR), radiometric intercalibration.**

I. Introduction

THE defense meteorological satellite program operational linescan system (DMSP-OLS) has a powerful photoelectric amplification and gain, and it can detect electromagnetic waves emitted by city lights, lightning, and fire [1]–[4]. DMSP-OLS night-time light (NTL) imageries have been widely and successfully implemented in studying human activity [5], e.g., the evolution of urban spatial patterns [6]–[12], the evaluation of the economic development level [13]–[19], the estimation of population density [20]–[24], the estimation of power consumption [25], [26], the assessment of carbon emission [27]–[29], and the study of the heat island effect [30]–[32], etc.

Unfortunately, DMSP-OLS products have some drawbacks due to many factors (e.g., the atmospheric absorption, scattering, solar altitude angle, sensor calibration, and terrain illumination) so that they are not calibrated well radiometrically. It is difficult to compare feedback from different dates within the same region [33]–[35]. Hence, a radiometric intercalibration to normalize DMSP-OLS imageries from different dates should be performed. In comparison with the absolute radiometric calibration, relative radiometric calibration (i.e., intercalibration) uses the radiometric information intrinsic to the images themselves and this alternative method has been widely used [36]–[41].

Accuracy and automation are the major problems with regards to the relative radiometric calibration, which are detailed as follows.

1) The calibration site selection of radiometric intercalibration: Calibrating image also requires a good distribution of the calibration sites. Zhang *et al.* [42] and Li *et al.* [38] utilized calibration sites to calibrate NTL imagery globally and regionally. Comparative experiments of the relative calibration (i.e., intercalibration) methods for DMSP-OLS NTL showed that global-scale calibration methods outperform regional-scale calibration methods [6], [43], [44]. Therefore, to obtain the best results, we also choose six regions all over the global world for calibration in this article.
2) The mathematical model selection of radiometric intercalibration: Due to model error, different models [44], [45], including linear model [38], [40], second-order polynomial model [42], [46]–[49], and sixth-order polynomial model [50], etc., were selected to intercalibrate the radiometric value of DMSP-OLS imagery. Although a high-order polynomial is widely selected as the model of imagery intercalibration, it may lead to the overparameterization problem [51]–[53] so that whether it is an optimal model or not needs testing. The manual operation of selecting a stable reference pixel is the way to study the optimal intercalibration model of the DMSP radiometric

Manuscript received October 2, 2020; revised December 23, 2020 and January 7, 2021; accepted January 11, 2021. Date of publication January 14, 2021; date of current version February 3, 2021. This work was supported in part by the National Key R&D Program of China under Grant 2019YFE0126800, in part by the National Natural Science Foundation of China under Grant 41771493 and Grant 41101407, in part by the Wuhan Youth Science and Technology Plan under Grant 2016070204010137, and in part by the self-determined research funds of CCNU from the basic research and operation of the MOE under Grant CCNU19TS002. *(Corresponding author: Chang Li.)*

Chang Li is with the Key Laboratory for Geographical Process Analyzing and Modeling, College of Urban and Environmental Science, Central China Normal University, Wuhan 430079, China (e-mail: lcshaka@126.com).

Xi Li is with the State Key Laboratory of Information Engineering in Surveying, Mapping, and Remote Sensing, Wuhan University, Wuhan 430072, China (e-mail: li_rs@163.com).

Tian Li is with the Johns Hopkins University, Baltimore, MD 21218 USA (e-mail: tli80@jh.edu).

Qi Meng and Wenjie Yu are with the College of Urban and Environmental Science, Central China Normal University, Wuhan 430079, China (e-mail: qimeng@ccnu.edu.cn; 739873271@qq.com).

Digital Object Identifier 10.1109/JSTARS.2021.3051800

intercalibration [39], which inspires us that it is necessary to control the model error. However, in this manual method, selecting the invariant regions is vulnerable to subjective cognition, which affects the accuracy of the results, and it is time consuming and labor intensive.

3) Accuracy evaluation and analysis of radiometric intercalibration: Many studies only or mainly use R^2 (coefficient of determination) to evaluate precision, which fails to ensure the accuracy of intercalibration fully as well as subjectively, and they always lack an explanation of the optimal model generation reasons, e.g., the most popular way to evaluate DMSP-OLS NTL imagery intercalibration model is R^2, which reflects relative precision rather than absolute accuracy; thus, the results lack objectivity. We have proposed the use of a more objective evaluation criterion, the absolute error [root-mean-square error (RMSE) and adjusted RMSE], to evaluate the performance of the algorithms [41]. Hence, we still recommend the use of these objective indicators for evaluation. Moreover, how to explain the reasons for the high accuracy of the intercalibration model is worth further study.
4) The automatic selection of reference pixels with a stable digital number (DN): Unstable DN can be regarded as a gross error, which leads to big errors and has a great impact on the correctness of the final intercalibration results. Based on ridgeline sampling regression [42] and robust regression [38], the semiautomatic and automatic algorithms are both effective in the radiometric intercalibration of NTL imagery, which enhances the imagery quality by radiometric intercalibration. For the full automatic methods, we have previously studied and compared least median of squares (LMedS), random sample consensus, posterior variance estimation, Danish method, and empirical rule for radiometric intercalibration to eliminate the variant pixels with the highest accuracy, stability, and efficiency. The final results where LMedS works best were proposed for the intercalibration of the radiometric values of NTL imagery using the adjusted RMSE evaluation criteria [41]. However, our previous methods only considered the problem of eliminating outliers (i.e., gross error) and used the simplest linear model to calibrate each other, instead of selecting an optimal model from multiple models by comparison (i.e., model error).

In general, the previous studies of DMSP-OLS NTL imagery intercalibration either focused on a discussion of how to automatically select pixel values or addressed the optimal intercalibration model. They failed to explain the generation reason for the optimal model or to systemically evaluate the radiometric intercalibration of automation, accuracy, and running speed. Hence, in view of the aforementioned literature, the following specific directions can be developed and improved further.

1) A radiometric intercalibration method to automatically process both model error and gross error for DMSP-OLS NTL imagery should be investigated, i.e., currently, there is a lack of an optimal model of radiometric intercalibration with automatically obtaining stable pixels for DMSP-OLS NTL imagery.
2) The reason for the optimal model of radiometric intercalibration for DMSP-OLS NTL imagery needs to be discussed and explained. Unfortunately, no article reported it.
3) The algorithm evaluation of the radiometric intercalibration for DMSP-OLS NTL imagery should take accuracy, automation, and speed of radiometric intercalibration together into account.

To solve the above-mentioned problems, this article proposes an optimal method of automatically radiometric intercalibration for DMSP-OLS NTL imagery by systematically studying and comparing five classic radiometric intercalibration models (i.e., linear, quadratic, power, exponential, and logarithmic regression) based on the automatic extraction of the reference pixels with stable lights. The innovation and contributions for this study are as follows.

1) An LMedS-based power regression (LBPR) is proposed for automatically radiometric intercalibration of DMSP-OLS NTL imagery for the first time. In order to select an optimal model and control both model error and gross error, the aforementioned five kinds of classical radiometric intercalibration model based on LMedS are the first to be studied and compared systematically.
2) The reason for the optimal model is the first to be methodically analyzed and explained from a mathematical point of view (e.g., Taylor expansion and probability principle).
3) The accuracy, automation, and speed of DMSP-OLS NTL imagery intercalibration are significantly improved. Currently, the proposed optimal model, LBPR, automatically controls the quality of data source errors (accidental error and gross error) and model errors (optimization model), without an artificial threshold. Finally, the accuracy, automation, and speed of intercalibration are optimized, which will lay the foundation for other related applications of the NTL remote sensing.

II. Methodology

In this study, we have used the LMedS algorithm to objectively explore the five frequently used regression models and exploit RMSE and adjusted RMSE to evaluate and analyze data results with the objective to obtain the optimal model (see Fig. 1 for the research approach).

In the imagery intercalibration processing, we can assume that there is a relationship between the pixel values of the image, which are collected by two different sensors from the same regions with stable lights. Moreover, the values can be linked with the intercalibration regression function f. Therefore, we have

$$(\mathrm{DN})_{\mathrm{Li}} = f\left[(\mathrm{DN})_{Ri}\right] \tag{1}$$

where $(\mathrm{DN})_{Ri}$ denotes the ith pixel DN in the right-hand slave image, which is obtained from the newer satellite sensors and used as the dependent variable, and $(\mathrm{DN})_{Li}$ denotes the ith pixel DN in the left-hand master image, which is obtained from the old sensors and used an independent variable. Then, using the regression function f fits the samples.

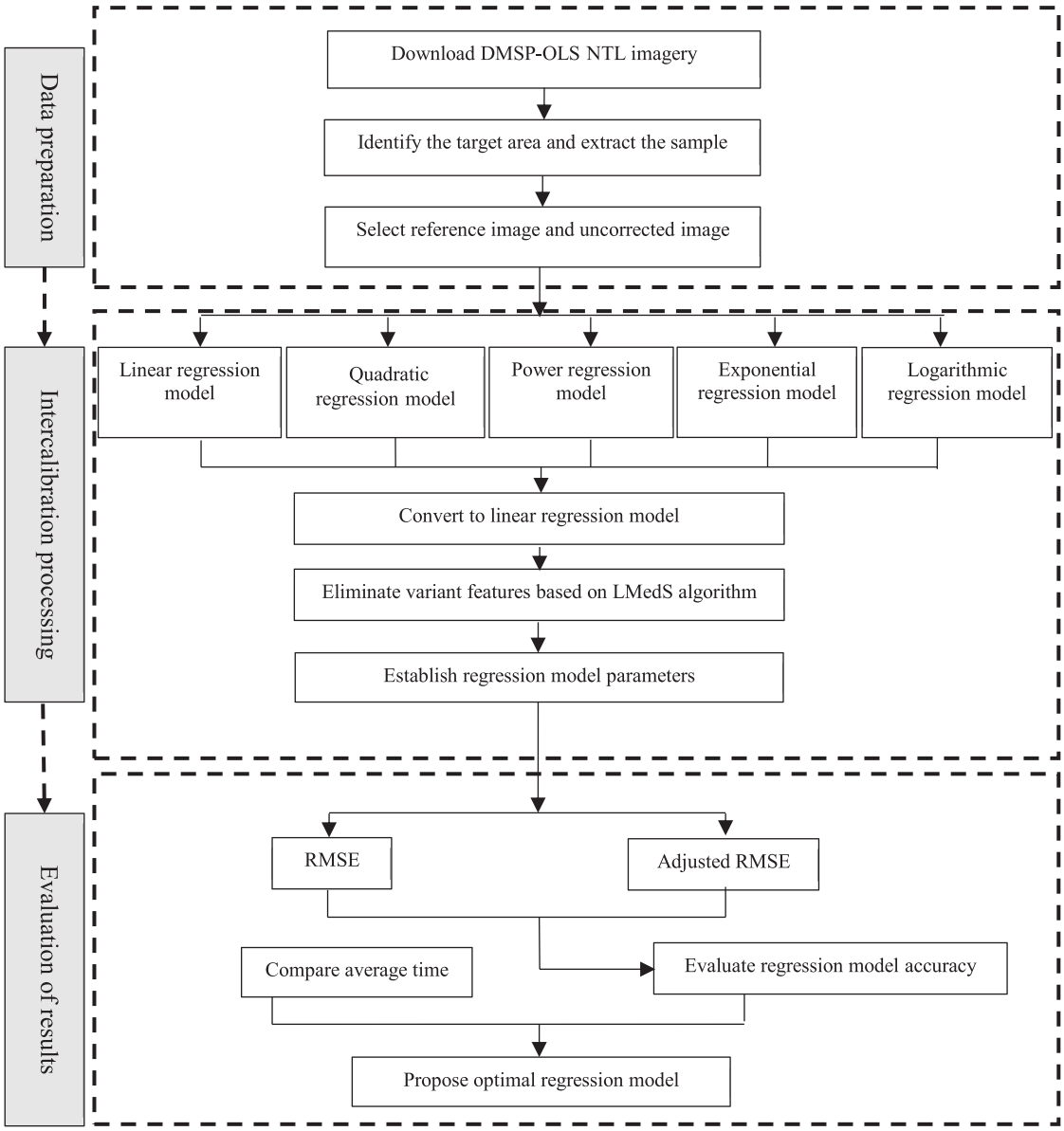

Fig. 1. Flowchart of the proposed intercalibration algorithm process.

A. Regression Models

Equation (1) can be expressed as a Taylor series (i.e., the *k*th order Taylor polynomial). In addition, this Taylor polynomial can be an approximate linearization, so the linear regression is utilized to express the difference in the sensor sensitivity between DMSP-OLS satellites. Thus, we have

$$(\mathrm{DN})_L = K_1(\mathrm{DN})_R + K_0 \tag{2}$$

However, the Taylor expansion, i.e., formula (2), usualy causes a truncation error. So other nonlinear models need to be considered. If the intercalibration relation (1) is a power regression model, the next formula is satisfied by

$$(\mathrm{DN})_L + 1 = K_1[(\mathrm{DN})_R + 1]^{K_0} \tag{3}$$

where "+1" is to prevent the value of $(\mathrm{DN})_R$ from being zero. If the intercalibration relation (1) is an exponential regression model, the next formula is

$$(\mathrm{DN})_L = K_0 K_1^{(\mathrm{DN})_R} \tag{4}$$

If the intercalibration relation (1) is a logarithmic regression model, the next formula is

$$(\mathrm{DN})_L = K_0 + K_1 \ln(\mathrm{DN})_R \tag{5}$$

where K_0 and K_1 from (2)–(5) denote the coefficients of the linear regression equation, power regression, exponential regression, and logarithmic regression, respectively. Actually, (3)–(5) can be converted to (2), so (2)–(5) can be rewritten in the matrix notation as

$$\begin{pmatrix} (DN)'_{L0} \\ (DN)'_{L1} \\ \vdots \\ (DN)'_{Ln} \end{pmatrix} = \begin{pmatrix} (DN)'_{R0}1 \\ (DN)'_{R1}1 \\ \vdots \\ (DN)'_{Rn}1 \end{pmatrix} \begin{pmatrix} K'_1 \\ K'_0 \end{pmatrix} \tag{6}$$

where $\mathbf{D}=[((\mathrm{DN})'_{R0},(\mathrm{DN})'_{R1},\ldots,(\mathrm{DN})'_{Rn})^T,(1,1,\ldots,1)^T]$, $\boldsymbol{x}=(K'_1,K'_0)^T$, $\boldsymbol{H}=((\mathrm{DN})'_{L0},(\mathrm{DN})'_{L1},\ldots,(\mathrm{DN})'_{Ln})^T$, and the "symbol ' " in the equation means variables after linearization transformation.

Moreover, when (1) is expanded to include the second-order terms according to the Taylor expansion, we can obtain a quadratic polynomial. Therefore, we have

$$(\mathrm{DN})_L = K_2(\mathrm{DN})_R^2 + K_1(\mathrm{DN})_R + K_0 \tag{7}$$

where K_0, K_1, and K_2 denote the coefficients of the quadratic polynomial regression equation.

Equation (7) can be rewritten in the matrix notation as

$$\begin{pmatrix}(\mathrm{DN})_{L0}\\(\mathrm{DN})_{L1}\\\vdots\\(\mathrm{DN})_{Ln}\end{pmatrix}=\begin{pmatrix}(\mathrm{DN})_{R0}^2&(\mathrm{DN})_{R0}&1\\(\mathrm{DN})_{R1}^2&(\mathrm{DN})_{R1}&1\\&\vdots\\(\mathrm{DN})_{Rn}^2&(\mathrm{DN})_{Rn}&1\end{pmatrix}\begin{pmatrix}K_2\\K_1\\K_0\end{pmatrix} \tag{8}$$

where $\mathbf{D}=\begin{bmatrix}(\mathrm{DN})_{R0}^2&(\mathrm{DN})_{R0}&1\\(\mathrm{DN})_{R1}^2&(\mathrm{DN})_{R1}&1\\\vdots&\vdots&\vdots\\(\mathrm{DN})_{Rn}^2&(\mathrm{DN})_{Rn}&1\end{bmatrix}$, $\boldsymbol{x}=(K_2,K_1,K_0)^T$, and $\boldsymbol{H}=((\mathrm{DN})_{L0},(\mathrm{DN})_{L1},\ldots(\mathrm{DN})_{Ln})^{\mathrm{T}}$.

Then, (6) and (8) can be unified as

$$\boldsymbol{H}=\mathbf{D}\boldsymbol{x} \tag{9}$$

However, both sides of (9) are not exactly equal, so we let $\boldsymbol{E}$ be the residual vector. The standard least squares method is used to minimize $\boldsymbol{E}$

$$\boldsymbol{E}=\mathbf{D}\boldsymbol{x}-\boldsymbol{H} \tag{10}$$

Selecting the best model from the above-mentioned models can reduce the model error. Then, the following section will describe how to eliminate gross errors.

B. Least Median of Squares

In our previous work, we showed that the LMedS method [54], [55], which can randomly estimate the parameters, is the optimal algorithm with the highest accuracy for the automatically radiometric intercalibration of DMSP-OLS imagery [41]. Hence, this study only proposes the LMedS to automatically remove the gross errors of the above-mentioned five frequently used types of regression on the intercalibration models and to achieve the highest accuracy of radiometric intercalibration. If we take the gross errors (i.e., unstable NTL pixels) into account, weighted least squares (WLS) can be written as

$$\boldsymbol{E}^T\mathbf{P}\boldsymbol{E}=\min \tag{11}$$

where **P** is the weighted matrix. The final objective function of LMedS is

$$\min\ \left(\underset{i}{\mathrm{med}}\ E_i^2\right) \tag{12}$$

where E_i is the *i*th residual error of the *i*th observation in the aforementioned regression equation, including five kinds of algorithm, i.e., LMedS-based linear regression (LBLR), LMedS-based quadratic regression (LBQR), LBPR, LMedS-based exponential regression (LBER), and LMedS-based logarithmic regression (LBLoR). When obtaining the minimal median, the final coefficients of the regression equation can be calculated by WLS

$$p_i=\begin{cases}1 & \text{if } E_i<1.4826\left[1+5/(n-t)\right]\sqrt{M_j}\\0 & \text{otherwise}\end{cases} \tag{13}$$

where M_j is the minimal median. If $p_i=0$, it means that the *i*th observation is an unstable pixel (i.e., gross error). So, $P=\mathrm{diag}(p_1,\ \ldots,p_n)$. The solution of the equation is

$$\boldsymbol{x}=\left(\mathbf{D}^T\mathbf{P}\mathbf{D}\right)^{-1}\mathbf{D}^T\mathbf{P}\boldsymbol{H} \tag{14}$$

However, in the random sampling of LMedS, it is pertinent to note that in the calculation of a quadratic polynomial based on LMedS, the singular or ill-conditioned matrix is likely to appear, so the matrix should be tested. At each time step, three points of the DN value are randomly sampled using LMedS; then, we can obtain

$$\mathbf{A}=\begin{pmatrix}(\mathrm{DN})_{Ri}^2(\mathrm{DN})_{Ri}1\\(\mathrm{DN})_{Rj}^2(\mathrm{DN})_{Rj}1\\(\mathrm{DN})_{Rk}^2(\mathrm{DN})_{Rk}1\end{pmatrix} \tag{15}$$

To determine whether it is an ill-conditioned matrix or not, we can use a condition number

$$K(\mathbf{A})=\|\mathbf{A}\|\left\|\mathbf{A}^{-1}\right\| \tag{16}$$

There are multiple approaches for the matrix paradigm $\|\bullet\|$, such as one-paradigm, two-paradigm, and so on. We choose two-paradigm as a computational method, and $||\mathrm{A}||=\sqrt{\lambda_1}$, where λ_1 is the maximum eigenvalue of $\mathbf{A}^T\mathbf{A}$, when one of the following is true:

$$K(\mathbf{A})\ \geq 10^{10} \tag{17}$$

$$\det(\mathbf{A})\ =0 \tag{18}$$

It can be identified as an ill-conditioned matrix so that the sampling is invalid and needs to be resampled randomly. Furthermore, on the basis of our previous investigations [51]–[53], the selection of high-order polynomial for both geometric and radiometric correction is very likely to lead to the overparameterization problem so that the accuracy of imagery correction is reduced. Actually, in the following experimental section, we can find that the intercalibrated accuracy of quadratic regression is the last but one due to overparameterization problem. Therefore, higher order ($\geq$3) polynomials are not selected for imagery intercalibration in this article

C. Evaluation of Results

Different from widely used R^2 that is as a relative error but fails to evaluate how close the calibration value is to the actual value, RMSE, as an absolute error that can measure the deviation between the referenced true value and the calibrated

value, is usually used for the accuracy evaluation of radiometric intercalibration for DMSP-OLS imagery. However, the check data of the ROIs (i.e., cross validation) may have outliers (i.e., variant light pixels), even if it is selected by manual operation. Thus, to solve the above-mentioned issue, the adjusted RMSE [41] is used by calculating

$$\text{Adjusted RMSE} = \sqrt{\frac{1}{M-\alpha}\sum_{j=\alpha/2+1}^{M-\alpha/2}[\text{Er}(j)]^2} \quad (19)$$

where α/M is the outlier percentage, "Prob" means the probability or frequency, and Er (j) is the sort result in the nondecreasing order with the no. j.

This article utilizes RMSE, adjusted RMSE, and running speed to evaluate the performance of the five types of common regression models based on the LMedS algorithm. It is worth noting that R^2 is not an important indicator for the evaluation of experimental results and not used because it represents the relative precision and its index reflects an internal precision and is similar to the overfitting problem with low accuracy in machine learning.

III. Experimental Results and Analysis

A. Data Sources

1) DMSP-OLS data: The performance of the proposed methods is tested using annual NTL data from the website of the National Geophysical Data Center.[1] In view of the fact that only one satellite image was produced over the years, it does not meet the requirements of the intercalibration and shortens the continuity of the study. This article encompasses data for 12 years, from 1994 and 1997 to 2007. DMSP imagery is raster image data, the reference system is the WGS-84 coordinate system, the spectral resolution is 6 bit, and the gray value range is 0–63.
2) Geographical data of the world: This article utilizes the geographical data of the world's national administrative division from the Diva GIS platform. With the purpose of matching the DMSP image data, the reference system of the geographical data is also set to the WGS-84 coordinate system.[2]

B. Study Areas

In this article, the NTL imagery dataset contains imageries that are obtained from four different DMSP satellites, namely, F10 (1994), F12 (1994 and 1997–1999), F14 (1997–2003), F15 (2000–2007), and F16 (2004–2007). During the period from 1997 to 2007, the NTL data in the selected areas were provided by two different DMSP satellites so that the radiometric values of imagery could be intercalibrated.

This study also takes the following conditions into account.

1) The selected region should be located in different regions, with a global representation.
2) The selected area is moderate in size.

[1][Online]. Available: http://ngdc.noaa.gov/eog/dmsp/downloadV4composites.html

[2][Online]. Available: www.diva-gis.org/Data

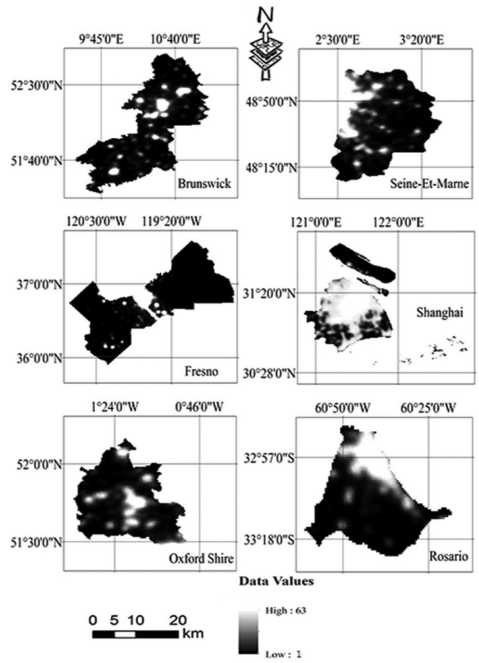

Fig. 2. DMSP imageries of the study regions.

3) Each country's administrative division system is different, so the data are extracted according to the second-grade administrative division of the country.

Given these conditions, the final chosen experimental areas are the Seine-Et-Marne of France, Oxford County of England, the city of Brunswick in Germany, the city of Shanghai in China, the city of Fresno in the United States, and the city of Rosario in Argentina (the study area is shown in Fig. 2).

C. Data Processing

Based on the ArcGIS platform, a total of 22 global phase DMSP image data were extracted from the six selected areas using the WGS-84 coordinate system and the Lambert azimuthal equal area projection in order to reduce the distortion in the area. The grid property tool in the data management module is applied to create the raster data property sheet and to extract the bright value imagery.

To improve the efficiency of the intercalibration, it is not necessary to build the intercalibration regression (i.e., LBLR, LBQR, LBPR, LBER, and LBLoR) using all of the pixels in the regions. Thus, the samples were evenly and randomly selected as ROIs to obtain the control DN values about 30%–40% of the total pixels. Except for those ROIs, the rest of the samples about 60%–70% of the total pixels were selected as checking areas to assess the accuracy of the evaluation. It is worth noting that all the samples of NTL saturated pixels and zero value pixels should be avoided.

Using the Matlab platform, the control data of the ROIs are input to calculate the parameters and relative error. Then, the check data of the ROIs (cross validation) are carried out for the absolute error test. Finally, we evaluate the advantages and

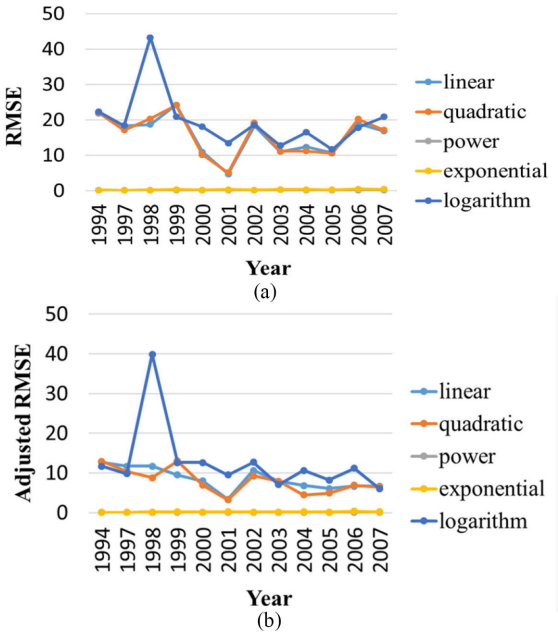

Fig. 3. Comparison of the absolute error with a relative error of the five regression models for radiometric intercalibration in Brunswick from 1994 and 1997 to 2007. (a) RMSE of Brunswick. (b) Adjusted RMSE of Brunswick.

disadvantages of each regression model and choose the optimal model.

The software and hardware platform used in this experiment are listed as follows:

1) CUP: Intel Core i5-4210M;
2) RAM: 4 GB;
3) ArcMap: 10.2;
4) Matlab: R2012a; and
5) Operating system: Windows 10 professional 64 bit.

D. Performance Evaluation and Analysis of Results

In the experiments, we evaluated and compared five frequently used regression models by using RMSE, adjusted RMSE, and the running speed, based on the DMSP datasets of the six regions selected over the world. As given in Table I and Figs. 3–11, the results are as follows.

1) From Table I and Figs. 3–8(a) and (b), it can be found that the variation trends of RMSE and adjusted RMSE are generally consistent for the five regression models. Because the absolute error is a very objective evaluation method, these evaluation indicators are similar and can even be approximately equivalent under some certain conditions. However, in some cases, the variance of the RMSE and the adjusted RMSE of the logarithm regression model is inconsistent. For example, the Brunswick region in 2005–2007 is inconsistent, as shown in Fig. 3. In some inconsistent years, Fig. 4 shows that the evaluations of the RMSE and adjusted RMSE achieve consistent sorting results in 2000 and 2002.
2) The findings of absolute error and relative error are inconsistent. Due to the definition of accuracy and precision, we know that the essence of relative error (e.g., R^2) refers

TABLE I
RESULTS OF THE PERFORMANCE EVALUATION OF INTERCALIBRATION MODELS IN SHANGHAI

Year	Model	RMSE	Adjusted RMSE
1994	linear	10.92	6.36
	quadratic	12.64	8.12
	power	0.06	0.03
	exponential	0.05	0.03
	logarithm	8.84	3.92
1997	linear	11.67	9.54
	quadratic	12.23	10.37
	power	0.06	0.05
	exponential	0.056	0.04
	logarithm	10.86	9.82
1998	linear	23.58	19.82
	quadratic	13.78	10.06
	power	0.24	0.18
	exponential	0.36	0.29
	logarithm	14.19	9.55
1999	linear	11.44	7.10
	quadratic	12.99	8.77
	power	0.12	0.07
	exponential	0.14	0.08
	logarithm	14.25	9.47
2000	linear	8.47	4.12
	quadratic	7.10	3.59
	power	0.14	0.09
	exponential	0.11	0.08
	logarithm	14.33	8.07
2001	linear	14.02	7.35
	quadratic	14.01	7.52
	power	0.26	0.12
	exponential	0.26	0.14
	logarithm	16.96	11.44
2002	linear	14.59	7.63
	quadratic	14.07	7.05
	power	0.17	0.11
	exponential	0.17	0.09
	logarithm	13.87	8.78
2003	linear	13.01	7.48
	quadratic	11.46	6.02
	power	0.14	0.09
	exponential	0.32	0.28
	logarithm	14.38	9.63
2004	linear	16.20	11.78
	quadratic	16.60	11.83
	power	0.15	0.11
	exponential	0.57	0.42
	logarithm	22.42	17.77
2005	linear	13.73	9.24
	quadratic	13.44	8.62
	power	0.14	0.09
	exponential	0.22	0.17
	logarithm	12.85	6.77
2006	linear	14.71	9.48
	quadratic	12.67	9.03
	power	0.14	0.07
	exponential	0.10	0.07
	logarithm	29.50	12.39
2007	linear	10.84	6.39
	quadratic	10.44	6.20
	power	0.09	0.05
	exponential	0.10	0.06
	logarithm	11.20	7.52

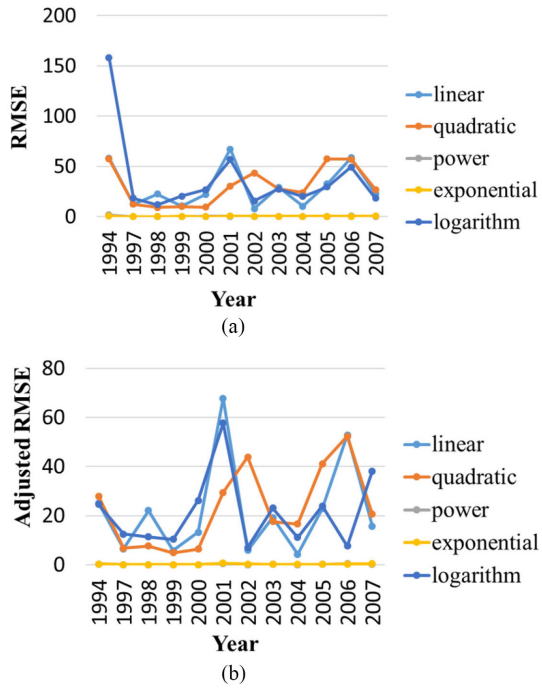

Fig. 4. Comparison of the absolute error with a relative error of the five regression models for radiometric intercalibration in Rosario from 1994 and 1997 to 2007. (a) RMSE of Rosario. (b) Adjusted RMSE of Rosario.

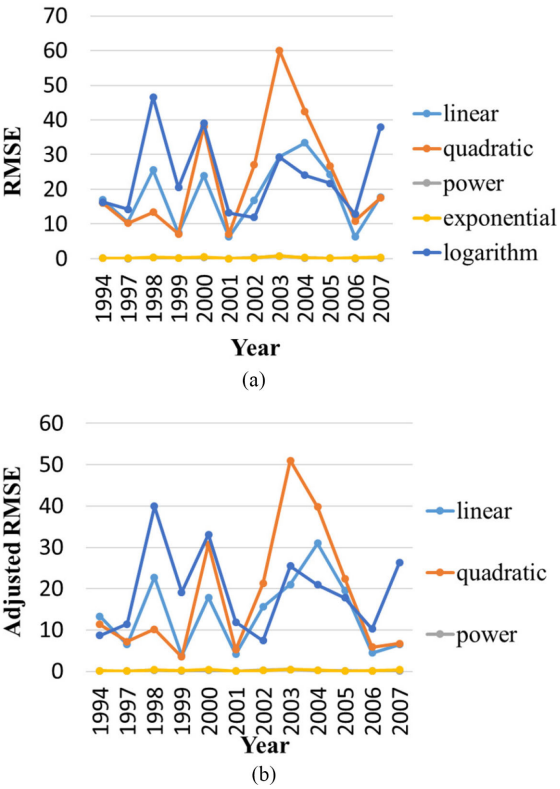

Fig. 5. Comparison of the absolute error with a relative error of the five regression models for radiometric intercalibration in Oxford Shire from 1994 and 1997 to 2007. (a) RMSE of Oxford Shire. (b) Adjusted RMSE of Oxford Shire.

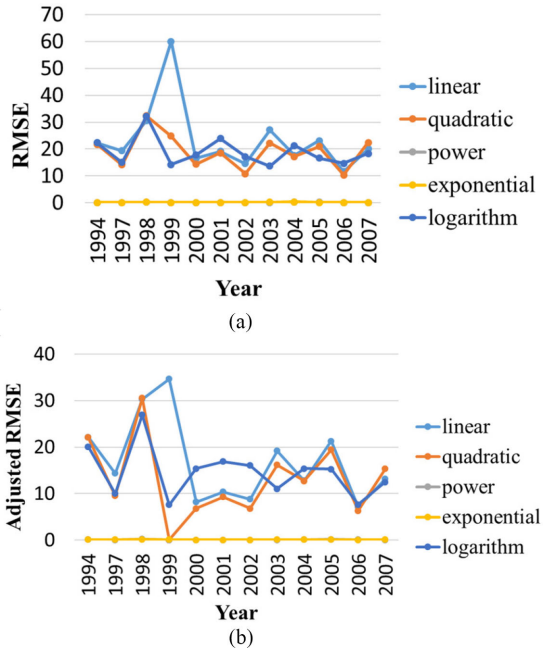

Fig. 6. Comparison of the absolute error with a relative error of the five regression models for radiometric intercalibration in Seine-Et-Marne from 1994 and 1997 to 2007. (a) RMSE of Seine-Et-Marne. (b) Adjusted RMSE of Seine-Et-Marne.

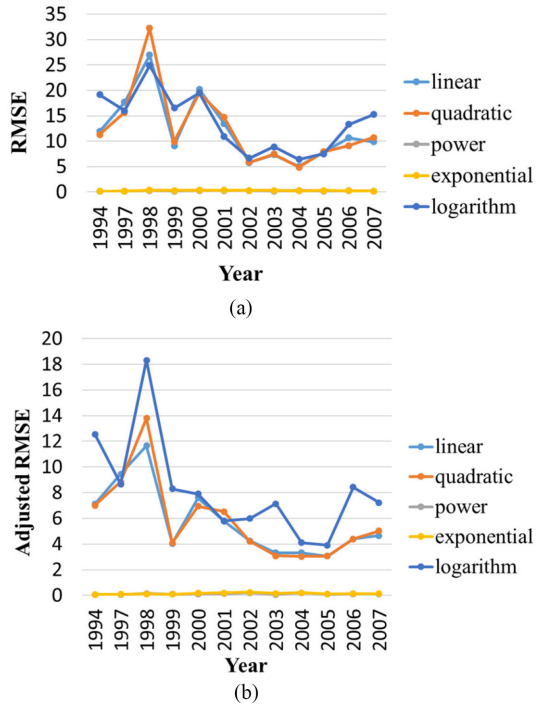

Fig. 7. Comparison of the absolute error with a relative error of the five regression models for radiometric intercalibration in Fresno from 1994 and 1997 to 2007. (a) RMSE of Fresno. (b) Adjusted RMSE of Fresno.

to precision, while the absolute error (e.g., RMSE and adjusted RMSE) refers to accuracy. Accuracy represents the difference between the measured value and the true value, and precision represents the dispersion degree of the distance between the results of a group or the reproducibility

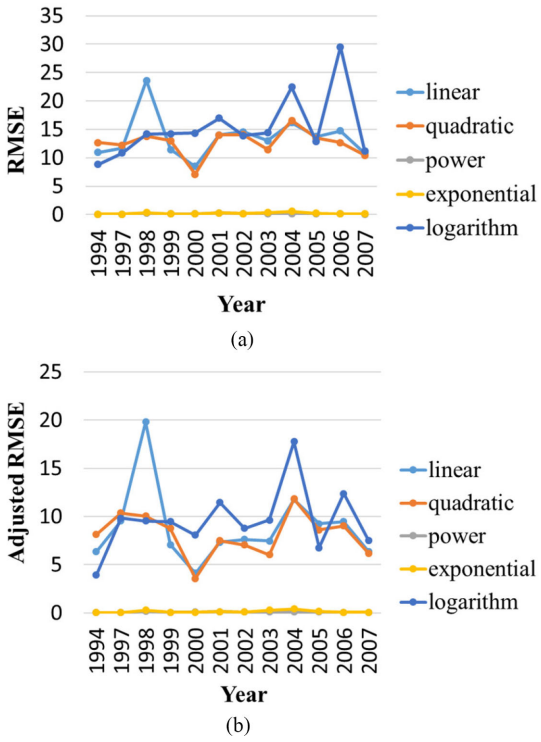

Fig. 8. Comparison of the absolute error with a relative error of the five regression models for radiometric intercalibration in Shanghai from 1994 and 1997 to 2007. (a) RMSE of Shanghai. (b) Adjusted RMSE of Shanghai.

of the measurement. Therefore, the regression model with the minimum relative error, namely, maximum correlation (R^2), does not always have the minimum absolute error, which is similar to the overfitting phenomenon with low predictive power in artificial intelligence. Comparing the absolute error and relative error in 1994 and 1997–2007, the LBPR and LBER have the minimum absolute errors but they have higher relative errors than the other three regression models (LBLR, LBQR, and LBLoR). When comparing the absolute error and relative error for the 12 years of data (as shown in Fig. 5), the LBER has the lowest absolute errors but it has higher relative errors in the regions.

3) The results of the five types of regression models based on the data calculated for 12 years were compared. As shown in Figs. 3–8, the absolute errors of the linear and exponential regression models are basically consistent and higher than the other three regression models. From Figs. 6–8, we find that the LBLR and the LBQR are consistent with the absolute error for 2000 to 2007. Compared with the total absolute error of the five regression models over the decade, the LBPR has the minimum error. In addition, we find that the LBLoR has the maximum absolute error, as shown in Fig. 9(a), (b), (e), (f), (i)–(l). The LBLR has the maximum absolute error, as shown in Fig. 9(g) and (h). In addition, the LBQR has the maximum absolute error, as shown in Fig. 9(c) and (d).
4) The findings from Figs. 3–8 and data for the five regression models indicate that the relative precision of the LBPR

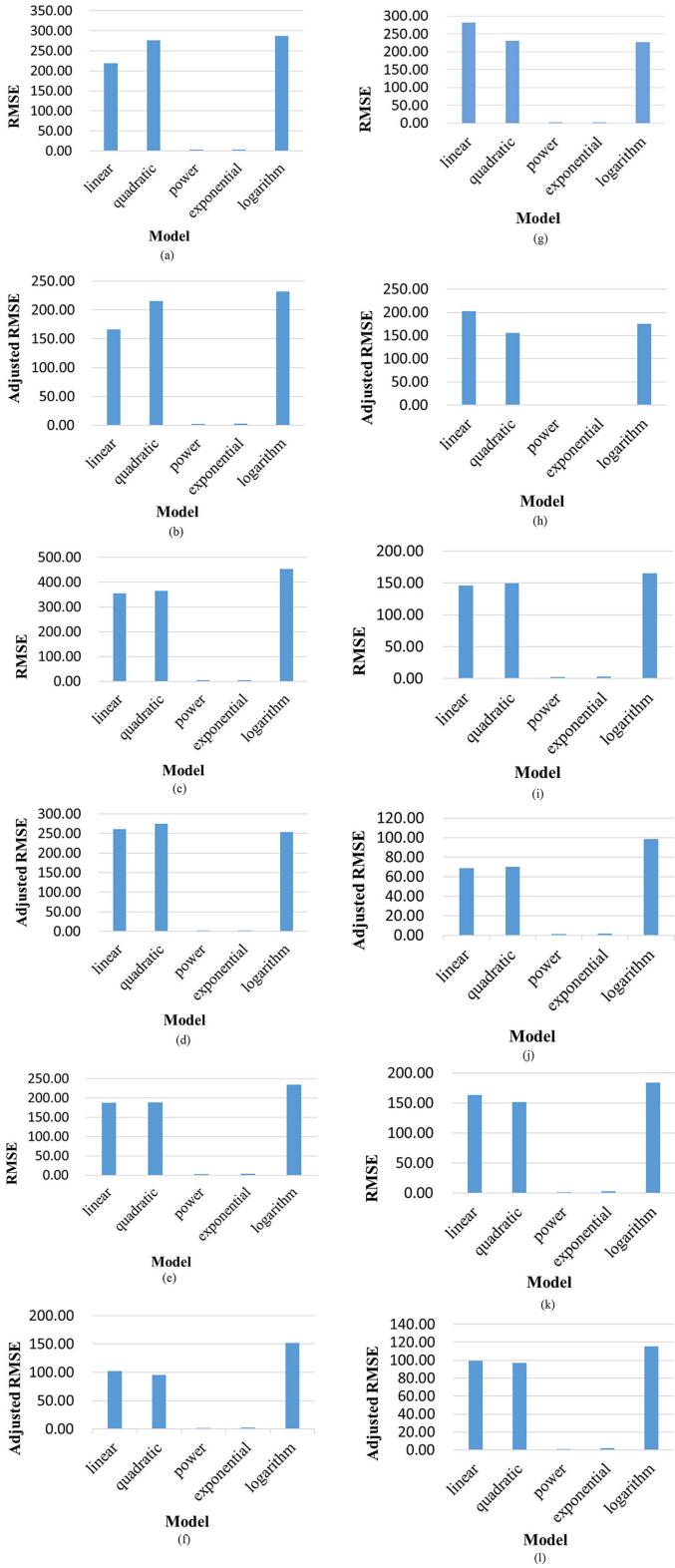

Fig. 9. Comparison of the total absolute error of the five regression models for radiometric intercalibration for 12 years of data. (a) Total RMSE of Oxford Shire in 12 years. (b) Total adjusted RMSE of Oxford Shire in 12 years. (c) Total RMSE of Rosario in 12 years. (d) Total adjusted RMSE of Rosario in 12 years. (e) Total RMSE of Brunswick in 12 years. (f) Total adjusted RMSE of Brunswick in 12 years. (g) Total RMSE of Seine-Et-Marne in 12 years. (h) Total adjusted RMSE of Seine-Et-Marne in 12 years. (i) Total RMSE of Fresno in 12 years. (j) Total adjusted RMSE of Fresno in 12 years. (k) Total RMSE of Shanghai in 12 years. (l) Total adjusted RMSE of Shanghai in 12 years.

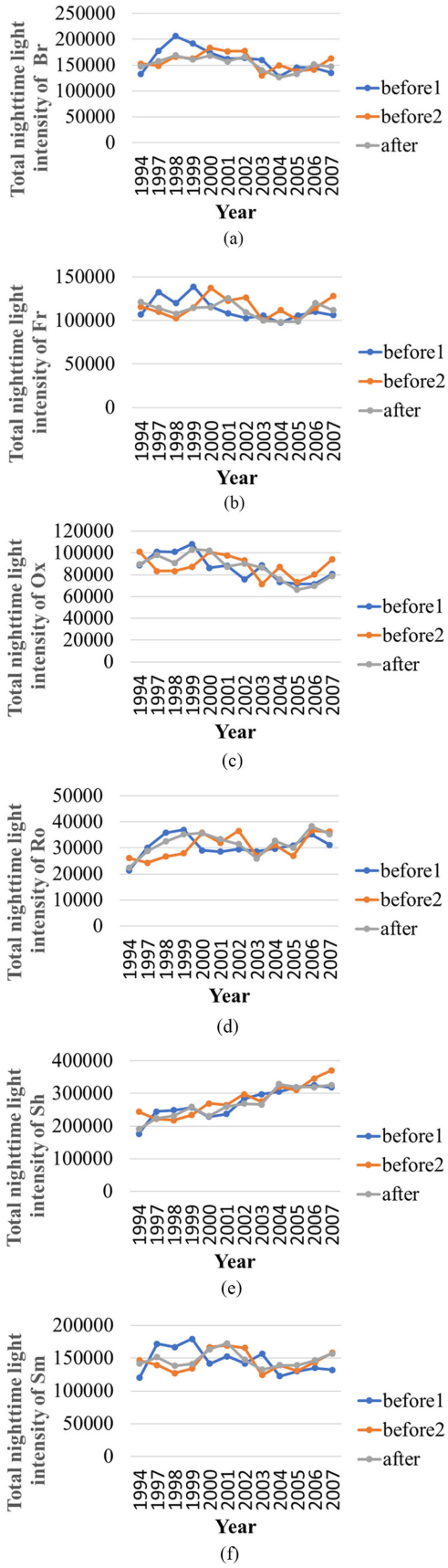

Fig. 10. Each year's TNLI before and after intercalibration based on LBPR over 12 years. (a)–(f) Corresponding Brunswick, Fresno, Oxford, Rosario, Shanghai, and Seine-Et-Marne.

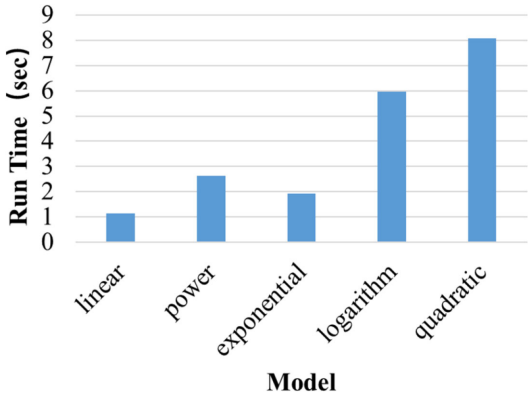

Fig. 11. Comparison of the running speed of the five regression models for radiometric intercalibration over 12 years.

is similar to that of the LBQR and is much greater than those of other regression models; however, the LBER and LBLoR are less precise than other regression models.

5) The total nighttime light intensity (TNLI) of six cities before and after intercalibration based on LBPR over 12 years is showed in Fig. 10. Before intercalibration, there are two TNLIs corresponding to two satellites each year. After intercalibration, we can find that the results of TNLI on the time series are smoother than those before intercalibration.
6) The processing times of all the regression models are shown in Fig. 11. It can be seen that the average running speed of the LBLR is the fastest and the LBQR is the slowest. Moreover, the average running speeds of the LBPR and LBER are similar. The average running speed of the LBER is slightly faster than LBPR, and the average speed of LBLoR is faster than that of the LBQR.

E. Discussion

The experimental results show that the LBPR has the highest accuracy, and the LBLoR has the lowest accuracy. Meanwhile, the LBLR has the fastest running speed, the LBER and LBPR have the second and third fastest running speed, respectively, and the LBQR has the slowest running speed. Overall, the LBPR is the optimal model.

1) The accuracy of the LBPR is the best when comparing the accuracy of each regression. The calibration relation is based on a generalized relationship of radiometric intercalibration (1) and it can be carried out by the Taylor polynomial expansion, which is finite or infinite. When the power of the regression model is a positive integer, the second term expands to a finite term, for example, when the power is two, the power regression not only can generalize once to a second-order polynomial but also can even generalize to a polynomial of a higher order. When the power is not a positive integer, the Taylor expansion is an infinite term. In summary, the power regression used in this article can yield a polynomial of any order by the binomial theorem. The Taylor expansion principle shows that it can flexibly and maximally approximate

the intercalibration (1), so it has the highest accuracy. However, the linear regression model and the quadratic regression model can be regarded as the lower order Taylor expansions of the intercalibration (1), ignoring the higher order remainder, which leads to a larger truncation error. The Taylor polynomial expanded from the exponential regression model is infinite so that the fit is very good and is similar to the power regression. However, if the Taylor polynomial of the intercalibration (1) is finite, the exponential regression model will be overparameterized in the fitting so that the accuracy is reduced; thus, the absolute error of the exponential regression model is slightly lower than that of the power regression model. Therefore, the power regression model has the highest accuracy among the five models tested in this article. In addition, the aging of the photoelectric sensor is usually subject to an exponential distribution [56], and the brightness of the same image element is lowered as the sensor ages. According to the law of probability and statistics, the age distribution of many electronic products generally obeys an exponential distribution. In addition, the life distribution of some systems can be approximated by an exponential distribution, so the accuracies of the exponential regression model and power regression model are obviously superior to those of other regression models.

2) The results of the comparison between absolute error and relative error show that the LBLoR is the least accurate in the calculation of radiometric intercalibration, which is due to the characteristic of the logarithmic regression model. This model needs to pass the fixed point, taking (15) as an example, as a fixed point $(1, K_0)$, which is a difficult criterion to meet in the actual intercalibration relation. In addition, the logarithmic regression is usually the inverse of the exponential regression; thus, if the intercalibration model conforms to the exponential regression, it will not conform to the (inverse) logarithmic regression. Therefore, the regression model is the least accurate model. Moreover, the absolute error shows that the LBQR is the last but one due to the overparameterization problem. It is worth noting that according to the International Organization for Standardization (ISO) 5725-1 1994 [57], the precision (i.e., relative error) is the closeness of agreement among a set of results so that it is not the most effective way of expressing error. Accuracy (i.e., absolute error) is used to describe the closeness of a measurement to the true value so that it is a direct and effective way of expressing error. Hence, the higher R^2 does not mean the true error is smaller. Since the overparameterization or overfitting problem exists in high-order (≥ 2) polynomials, they are not suitable for the radiometric intercalibration of DMSP-OLS NTL imagery.
3) By comparing the average run times of the five kinds of models, we know that the LBLR runs the fastest, as its run time is determined by its computational complexity. The LBPR, LBER, and LBLoR all need to be linearized first and then treated as a linear regression. Moreover, the LBQR needs to be computed at three points at each time step by random sampling in the LMedS, and the pathological matrix examination is needed. In short, the computation of the aforementioned four models is more complicated than that of the linear regression model, so the linear regression model is the fastest. In addition, the quadratic model is much more cumbersome than the other four models, so it runs the slowest.
4) The LBPR should be developed further to harmonize DMSP-OLS and the visible infrared imaging radiometer suite (VIIRS). According to the existing high-quality papers, a logarithmic transformation and sigmoid function [58] for generating global DMSP NTL, a Gaussian low-pass filter [59] for spatial degradation, BFAST time-series decomposition, Lomb–Scargle periodogram, and geographically weighted regression [60] will be studied for the cross-sensor calibration.

Above all, considering the factors of accuracy and running speed, the LBPR has the highest accuracy and preferable running speed, so the LBPR is proposed as the optimal model. Moreover, the potential of LBPR needs to be mined and developed for cross-sensor (i.e., DMSP-OLS and VIIRS) calibration in the future.

IV. Conclusion and Future Work

In this study, on the basis of the LMedS that can automatically eliminate outliers and select stable reference pixel elements, comprehensive evaluating indicators, i.e., absolute error (RMSE and adjusted RMSE) and running speed, are adopted. After the radiometric intercalibration of the DMSP data from 1994 and 1997 to 2007 from different satellites in six regions over the global world, the operation is carried out for five elementary regression models. The experimental results show that the LBPR has the highest accuracy and a preferable running speed; therefore, the LBPR is the optimal model when both the accuracy and running speed of radiometric intercalibration are considered comprehensively for DMSP-OLS imagery. Furthermore, the mechanism why LBPR is an optimal method is explained.

The linear regression model and quadratic polynomial have long been empirically selected. However, this article provides another objective, an effective and automatically radiometric intercalibration model and method, LBPR, for the future study of radiometric intercalibration for DMSP imagery.

However, there is still room for further improvement in the accuracy of global DSMP-OLS data. Although the DN saturation overflow pixels of the DSMP-OLS dataset are removed as outliers so that there is no effect on the final intercalibration, how to modify the DN pixels of the DSMP-OLS saturation overflow will be the focus of future research.

Acknowledgment

The authors would like to thank for the comments and contributions of the editors, anonymous reviewers and the members of the editorial team.

REFERENCES

[1] T. A. Croft, "Nighttime images of the earth from space," *Sci. Amer.*, vol. 239, no. 1, pp. 86–101, 1978.

[2] C. D. Elvidge, K. E. Baugh, J. B. Dietz, T. Bland, P. C. Sutton, and H. W. Kroehl, "Radiance calibration of DMSP-OLS low-light imaging data of human settlements," *Remote Sens. Environ.*, vol. 68, no. 1, pp. 77–88, 1999.

[3] C. D. Elvidge *et al.*, "Night-time lights of the world: 1994–1995," *ISPRS J. Photogram. Remote Sens.*, vol. 56, no. 2, pp. 81–99, 2001.

[4] N. Levin *et al.*, "Remote sensing of night lights: A review and an outlook for the future," *Remote Sens. Environ.*, vol. 237, 2020, Art. no. 111443.

[5] M. Zhao *et al.*, "Applications of satellite remote sensing of nighttime light observations: Advances, challenges, and perspectives," *Remote Sens.*, vol. 11, no. 17, p. 1971, 2019.

[6] C. Small, F. Pozzi, and C. D. Elvidge, "Spatial analysis of global urban extent from DMSP-OLS night lights," *Remote Sens. Environ.*, vol. 96, no. 3/4, pp. 277–291, 2005.

[7] R. I. McDonald, P. Kareiva, and R. T. T. Forman, "The implications of current and future urbanization for global protected areas and biodiversity conservation," *Biol. Conservation*, vol. 141, no. 6, pp. 1695–1703, 2008.

[8] C. P. Lo, "Urban indicators of china from radiance-calibrated digital DMSP-OLS nighttime images," *Ann. Assoc. Amer. Geographers*, vol. 92, no. 2, pp. 225–240, 2015.

[9] H. Lu, M. Zhang, W. Sun, and W. Li, "Expansion analysis of Yangtze river delta urban agglomeration using DMSP/OLS nighttime light imagery for 1993 to 2012," *ISPRS Int. J. Geoinf.*, vol. 7, no. 2, p. 52, 2018.

[10] M. Alahmadi and P. M. Atkinson, "Three-fold urban expansion in Saudi Arabia from 1992 to 2013 observed using calibrated DMSP-OLS nighttime lights imagery," *Remote Sens.*, vol. 11, no. 19, 2019, Art. no. 2266.

[11] J. Peng *et al.*, "Spatiotemporal evolution of urban agglomerations in China during 2000–2012: A nighttime light approach," *Landscape Ecol.*, vol. 35, no. 2, pp. 421–434, 2020.

[12] V. Tselios and D. Stathakis, "Exploring regional and urban clusters and patterns in Europe using satellite observed lighting," *Environ. Planning B, Urban Anal. City Sci.*, vol. 47, no. 4, pp. 553–568, 2020.

[13] C. N. H. Doll, J.-P. Muller, and C. D. Elvidge, "Night-time imagery as a tool for global mapping of socioeconomic parameters and greenhouse gas emissions," *AMBIO, J. Human Environ.*, vol. 29, no. 3, pp. 157–162, 2000.

[14] P. C. Sutton, C. D. Elvidge, and T. Ghosh, "Estimation of gross domestic product at sub-national scales using nighttime satellite imagery," *Int. J. Ecol. Econ. Statist.*, vol. 8, no. S07, pp. 5–21, 2007.

[15] T. Ghosh, P. Sutton, R. Powell, S. Anderson, and C. D. Elvidge, "Estimation of Mexico's informal economy using DMSP nighttime lights data," in *Proc. Joint Urban Remote Sens. Event*, 2009, pp. 1–10.

[16] M. Chaturvedi, T. Ghosh, and L. Bhandari, "Assessing income distribution at the district level for India using nighttime satellite imagery," *Proc. Asia-Pacific Adv. Netw.*, vol. 32, pp. 192–217, 2011.

[17] C. Li, G. Li, Y. Zhu, Y. Ge, H.-T. Kung, and Y. Wu, "A likelihood-based spatial statistical transformation model (LBSSTM) of regional economic development using DMSP/OLS time-series nighttime light imagery," *Spatial Statist.*, vol. 21, pp. 421–439, 2017.

[18] M. J. Andrade-Núñez and T. M. Aide, "The socio-economic and environmental variables associated with hotspots of infrastructure expansion in South America," *Remote Sens.*, vol. 12, no. 1, p. 116, 2020.

[19] J. Cao, Y. Chen, J. P. Wilson, H. Tan, J. Yang, and Z. Xu, "Modeling China's prefecture-level economy using VIIRS imagery and spatial methods," *Remote Sens.*, vol. 12, no. 5, p. 839, 2020.

[20] P. Sutton, D. Roberts, C. Elvidge, and H. Meij, "A comparison of nighttime satellite imagery and population density for the continental United States," *Photogram. Eng. Remote Sens.*, vol. 63, no. 11, pp. 1303–1313, 1997.

[21] P. Sutton, "Modeling population density with night-time satellite imagery and GIS," *Comput., Environ. Urban Syst.*, vol. 21, no. 3/4, pp. 227–244, 1997.

[22] L. Zhuo, T. Ichinose, J. Zheng, J. Chen, P. J. Shi, and X. Li, "Modelling the population density of China at the pixel level based on DMSP/OLS non-radiance-calibrated night-time light images," *Int. J. Remote Sens.*, vol. 30, no. 4, pp. 1003–1018, 2009.

[23] S. J. Anderson, B. T. Tuttle, R. L. Powell, and P. C. Sutton, "Characterizing relationships between population density and nighttime imagery for Denver, Colorado: Issues of scale and representation," *Int. J. Remote Sens.*, vol. 31, no. 21, pp. 5733–5746, 2010.

[24] P. Kumar *et al.*, "Modeling the luminous intensity of Beijing, China using DMSP-OLS night-time lights series data for estimating population density," *Phys. Chem. Earth, A/B/C*, vol. 109, pp. 31–39, 2019.

[25] C. D. Elvidge, K. E. Baugh, E. A. Kihn, H. W. Kroehl, E. R. Davis, and C. W. Davis, "Relation between satellite observed visible-near infrared emissions, population, economic activity and electric power consumption," *Int. J. Remote Sens.*, vol. 18, no. 6, pp. 1373–1379, 1997.

[26] S. Sahoo, P. K. Gupta, and S. K. Srivastav, "Comparative analysis between VIIRS-DNB and DMSP-OLS night-time light data to estimate electric power consumption in Uttar Pradesh, India," *Int. J. Remote Sens.*, vol. 41, no. 7, pp. 2565–2580, 2020.

[27] M. Raupach, P. J. Rayner, and M. Paget, "Regional variations in spatial structure of nightlights, population density and fossil-fuel CO_2 emissions," *Energy Policy*, vol. 38, no. 9, pp. 4756–4764, 2010.

[28] Y. Sun, S. Zheng, Y. Wu, U. Schlink, and R. P. Singh, "Spatiotemporal variations of city-level carbon emissions in China during 2000–2017 using nighttime light data," *Remote Sens.*, vol. 12, no. 18, 2020, Art. no. 2916.

[29] Y. Yue, L. Tian, Q. Yue, and Z. Wang, "Spatiotemporal variations in energy consumption and their influencing factors in China based on the integration of the DMSP-OLS and NPP-VIIRS nighttime light datasets," *Remote Sens.*, vol. 12, no. 7, 2020, Art. no. 1151.

[30] K. P. Gallo, J. D. Tarpley, A. L. McNab, and T. R. Karl, "Assessment of urban heat islands: A satellite perspective," *Atmos. Res.*, vol. 37, no. 1/3, pp. 37–43, 1995.

[31] Y. Zhang and J. Cheng, "Spatio-temporal analysis of urban heat island using multisource remote sensing data: A case study in Hangzhou, China," *IEEE J. Sel. Topics Appl. Earth Observ. Remote Sens.*, vol. 12, no. 9, pp. 3317–3326, Sep. 2019.

[32] J. Li, F. Wang, Y. Fu, B. Guo, Y. Zhao, and H. Yu, "A novel SUHI referenced estimation method for multicenters urban agglomeration using DMSP/OLS nighttime light data," *IEEE J. Sel. Topics Appl. Earth Observ. Remote Sens.*, vol. 13, pp. 1416–1425, Apr. 2020, doi: 10.1109/JSTARS.2020.2981285.

[33] C. D. Elvidge *et al.*, "A fifteen year record of global natural gas flaring derived from satellite data," *Energies*, vol. 2, no. 3, pp. 595–622, 2009.

[34] J. V. Henderson, A. Storeygard, and D. N. Weil, "Measuring economic growth from outer space," *Amer. Econ. Rev.*, vol. 102, no. 2, pp. 994–1028, 2012.

[35] Y. Tu, H. Zhou, W. Lang, T. Chen, X. Li, and B. Xu, "A novel cross-sensor calibration method to generate a consistent night-time lights time series dataset," *Int. J. Remote Sens.*, vol. 41, no. 14, pp. 5482–5502, 2020.

[36] Y. Du, P. M. Teillet, and J. Cihlar, "Radiometric normalization of multitemporal high-resolution satellite images with quality control for land cover change detection," *Remote Sens. Environ.*, vol. 82, no. 1, pp. 123–134, 2002.

[37] M. J. Canty, A. A. Nielsen, and M. Schmidt, "Automatic radiometric normalization of multitemporal satellite imagery," *Remote Sens. Environ.*, vol. 91, no. 3/4, pp. 441–451, 2004.

[38] X. Li, X. Chen, Y. Zhao, J. Xu, F. Chen, and H. Li, "Automatic intercalibration of night-time light imagery using robust regression," *Remote Sens. Lett.*, vol. 4, no. 1, pp. 45–54, 2013.

[39] J. Wu, S. He, J. Peng, W. Li, and X. Zhong, "Intercalibration of DMSP-OLS night-time light data by the invariant region method," *Int. J. Remote Sens.*, vol. 34, no. 20, pp. 7356–7368, 2013.

[40] F.-C. Hsu, K. E. Baugh, T. Ghosh, M. Zhizhin, and C. D. Elvidge, "DMSP-OLS radiance calibrated nighttime lights time series with intercalibration," *Remote Sens.*, vol. 7, no. 2, pp. 1855–1876, 2015.

[41] C. Li, J. Ye, S. Li, G. Chen, and H. Xiong, "Study on radiometric intercalibration methods for DMSP-OLS night-time light imagery," *Int. J. Remote Sens.*, vol. 37, no. 16, pp. 3675–3695, 2016.

[42] Q. Zhang, B. Pandey, and K. C. Seto, "A robust method to generate a consistent time series from DMSP/OLS nighttime light data," *IEEE Trans. Geosci. Remote Sens.*, vol. 54, no. 10, pp. 5821–5831, Oct. 2016.

[43] M. Henderson, E. T. Yeh, P. Gong, C. Elvidge, and K. Baugh, "Validation of urban boundaries derived from global night-time satellite imagery," *Int. J. Remote Sens.*, vol. 24, no. 3, pp. 595–609, 2003.

[44] B. Pandey, Q. Zhang, and K. C. Seto, "Comparative evaluation of relative calibration methods for DMSP/OLS nighttime lights," *Remote Sens. Environ.*, vol. 195, pp. 67–78, 2017.

[45] X. Li and Y. Zhou, "Urban mapping using DMSP/OLS stable night-time light: A review," *Int. J. Remote Sens.*, vol. 38, no. 21, pp. 6030–6046, 2017.

[46] Z. Liu, C. He, Q. Zhang, Q. Huang, and Y. Yang, "Extracting the dynamics of urban expansion in China using DMSP-OLS nighttime light data from 1992 to 2008," *Landscape Urban Planning*, vol. 106, no. 1, pp. 62–72, 2012.

[47] T. Ma, C. Zhou, T. Pei, S. Haynie, and J. Fan, "Quantitative estimation of urbanization dynamics using time series of DMSP/OLS nighttime light data: A comparative case study from China's cities," *Remote Sens. Environ.*, vol. 124, pp. 99–107, 2012.
[48] C. D. Elvidge, F.-C. Hsu, K. E. Baugh, and T. Ghosh, "National trends in satellite-observed lighting," in *Global Urban Monitoring and Assessment Through Earth Observation*. New York, NY, USA: Taylor & Francis, 2014, pp. 97–118.
[49] N. Zhao, Y. Zhou, and E. L. Samson, "Correcting incompatible DN values and geometric errors in nighttime lights time-series images," *IEEE Trans. Geosci. Remote Sens.*, vol. 53, no. 4, pp. 2039–2049, Apr. 2015.
[50] J. Bennie, T. W. Davies, J. P. Duffy, R. Inger, and K. J. Gaston, "Contrasting trends in light pollution across Europe based on satellite observed night time lights," *Sci. Rep.*, vol. 4, 2014, Art. no. 3789.
[51] C. Li and H. Xiong, "A geometric and radiometric simultaneous correction model (GRSCM) framework for high-accuracy remotely sensed image preprocessing," *Photogram. Eng. Remote Sens.*, vol. 83, no. 9, pp. 621–632, 2017.
[52] C. Li, X. Liu, Y. Zhang, and Z. Zhang, "A stepwise-then-orthogonal regression (STOR) with quality control for optimizing the RFM of high-resolution satellite imagery," *Photogram. Eng. Remote Sens.*, vol. 83, no. 9, pp. 611–620, 2017.
[53] C. Li, J. Liu, X. Wang, X. Liu, and Y. Wu, "Stepwise-then-intelligent algorithm (STIA) for optimizing remotely sensed image rectification," *Int. J. Remote Sens.*, vol. 39, no. 21, pp. 7350–7369, 2018.
[54] P. J. Rousseeuw, "Least median of squares regression," *J. Amer. Statist. Assoc.*, vol. 79, no. 388, pp. 871–880, 1984.
[55] S. Choi, T. Kim, and W. Yu, "Perfo rmance evaluation of RANSAC family," in *J. Comput. Vis.*, vol. 24, no. 3, pp. 271–300, 1997.
[56] L.-I. Tong, K. S. Chen, and H. T. Chen, "Statistical testing for assessing the performance of lifetime index of electronic components with exponential distribution," *Int. J. Qual. Rel. Manage.*, vol. 19, pp. 812–824, 2002.
[57] *Accuracy (Trueness and Precision) of Measurement Methods and Results—Part 2: Basic Method for the Determination of Repeatability and Reproducibility of a standard Measurement Method*, ISO Standard 5725-2:1994, 1994.
[58] X. Li, Y. Zhou, M. Zhao, and X. Zhao, "A harmonized global nighttime light dataset 1992–2018," *Sci. Data*, vol. 7, no. 1, 2020, Art. no. 168.
[59] X. Li, D. Li, H. Xu, and C. Wu, "Intercalibration between DMSP/OLS and VIIRS night-time light images to evaluate city light dynamics of Syria's major human settlement during Syrian civil war," *Int. J. Remote Sens.*, vol. 38, no. 21, pp. 5934–5951, 2017.
[60] Q. Zheng, Q. Weng, and K. Wang, "Developing a new cross-sensor calibration model for DMSP-OLS and Suomi-NPP VIIRS night-light imageries," *ISPRS J. Photogram. Remote Sens.*, vol. 153, pp. 36–47, 2019.

Chang Li received the Ph.D. degree in photogrammetry and remote sensing from Wuhan University, Wuhan, China, in 2009.

He is currently a Professor with the Key Laboratory for Geographical Process Analysing and Modelling, Wuhan, China, and College of Urban and Environmental Science, Central China Normal University, Wuhan, China. He has authored or coauthored more than 80 research articles, among them, more than 40 articles that are indexed by SCI/EI. He has been authorized six national invention patents in China (all as the first contributor) and four national software copyrights in China (all as the first contributor). His current research interests include photogrammetry, computer vision, remote sensing change detection, spatiotemporal data analysis and modeling, 3-D reconstruction and modeling, and geographic system simulation.

Dr. Li was the recipient of the Science and Technology Progress Award of Hubei Province, China (second class, as the first contributor), in 2019, Government of Hubei Province, China, and the Talbert Abrams Grand Award (as the first contributor), and Talbert Abrams Award First Honorable Mention (as the first contributor) by American Society of Photogrammetry and Remote Sensing, in 2020 and 2018, respectively.

Xi Li received the Ph.D. degree in photogrammetry and remote sensing from Wuhan University, Wuhan, China, in 2009.

He is currently an Associate Professor with the State Key Laboratory of Information Engineering in Surveying, Mapping, and Remote Sensing, Wuhan University, Wuhan. His research interests include physical modeling of night-time light as well as night-time light remote sensing applications.

Dr. Li is an Editorial Board Member of the *International Journal of Remote Sensing* and an International Consultant for Asian Development Bank.

Tian Li received the bachelor of natural sciences degree in geography from Central China Normal University, Wuhan, China, in 2018. She has been an Exchange Student and majored in geography education from Southern Utah University, Cedar City, UT, USA, in 2017. She majors in digital education, and is currently working toward the graduate degree with Johns Hopkins University, Baltimore, MD, USA.

From 2018 to 2020, she was a fulltime Geography Teacher and Headteacher with Zhengzhou No.1 Middle School.

Ms. Li was a recipient of the National Scholarships of 2014–2015 and 2015–2016, the Mingde Scholarship of 2014–2015 (6%), the Student of Future Educators Plan, the Honor Student of Southern Utah University for consecutive two times, the first prize of The Third Geography Science Exhibition Competition of Chinese Universities (state level), and the bronze award of The Third Internet Plus College Students Innovation and Entrepreneurship Competition (state level).

Qi Meng was born in Tai'an City, China. She received the B.Sc. degrees in geographic information science and mathematics and applied mathematics from Central China Normal University, Wuhan, China, in 2020.

Wenjie Yu was born in Wuhan, China, in 1999. He is currently working toward the B.S. degree in geographic information science from Central China Normal University, Wuhan, China.

His research interest includes the calibration of night-time light remote sensing and time series analysis of vegetation remote sensing.